Fundamental Thermal-Hydraulic Pulp Digester Model with Grade Transition

Sharad Bhartiya, Pascal Dufour, and Francis J. Doyle III
Dept. of Chemical Engineering, University of Delaware, Newark, DE 19716

A detailed fundamental model of a continuous pulp digester was developed for simulation and control. Most modeling efforts in the past had emphasized either reaction kinetics and energy transfer assuming a prescribed flow behavior or modeled digester hydraulics with simplified reaction kinetics. The well-known extended Purdue model was augmented by incorporating axial momentum transport, of which an immediate consequence is the ability to simulate chip level and its impact on the Kappa number profile, thus enhancing the ability to model chip compaction. Interaction between digester hydraulics and kinetics is illustrated via simulation examples, including scenarios that show incipient plugging of the digester vessel. Higher-order finite-difference methods were also used to reduce numerical dissipation and dispersion. The ability to describe chip velocities enables rigorous tracking of a transition front within the digester during feedstock grade transitions. The model explains operational difficulties encountered during hardwood to softwood transition.

Introduction

Pulping mills convert wood chips to pulp suitable for paper production by displacing lignin from cellulose fibers. The conversion is achieved through a combination of strategies involving thermal, chemical, and mechanical degradation of the wood chips. Continuous Kraft processes use large, vertical, tubular reactors called digesters where the chips react with an aqueous solution of sodium hydroxide and sodium sulfide, known as white liquor, at elevated temperature. Most continuous digesters consist of three basic zones: an impregnation zone, a cooking zone, and a wash zone. A single vessel digester is shown in Figure 1. White liquor and pre-steamed chips are introduced at the top of the digester into the impregnation zone where the liquor penetrates the wet chips. However, most of the delignification reaction occurs only after the two streams flow downward into the subsequent cooking zone, where the mixture is heated to reaction temperatures achieved by liquor circulation through external heaters. The spent liquor is withdrawn from the digester at extraction screens located at the end of the cook zone, while the cooked chips continue the downward journey to the wash zone. Here, the chips are washed by the countercurrent flow of cold, dilute liquor. This effectively quenches the delignification reaction. The quality of the resulting pulp is described by Kappa number, which is a measure of the residual lignin content. A typical control objective of digester operation is to minimize variation in the Kappa # from a prescribed value. Continuous digesters present challenging problems in modeling and control. From a modeling perspective, the interplay between heat, mass, and momentum transport during the thermal-hydraulic degradation of the wood chips creates rich dynamic behavior. For example, softening of the chips, as cooking proceeds, causes them to compact more densely, which in turn affects the chip velocity profiles.

The capital-intensive nature of the pulp and paper industry mandates the development of operating strategies that use enhanced control, soft-sensing, and fault diagnosis methodologies, which are usually predicated on availability of a process model. A significant effort has been directed to the development of first-principles models that describe the thermal-hydraulic degradation of wood chips in the continuous pulp digester. Most fundamental continuous digester models in literature can be classified into two broad categories depending on the attributes they emphasize: (1) pulping chemistry; (2) hydraulic description of the chip and liquor streams.

Correspondence concerning this article should be addressed to F. J. Doyle, III at this current address: Dept. of Chemical Engineering, University of California-Santa Barbara, Santa Barbara, CA 93106.
Current address of S. Bhartiya: Dept. of Chemical Engineering, IIT, Bombay, Mumbai 400 076, India.

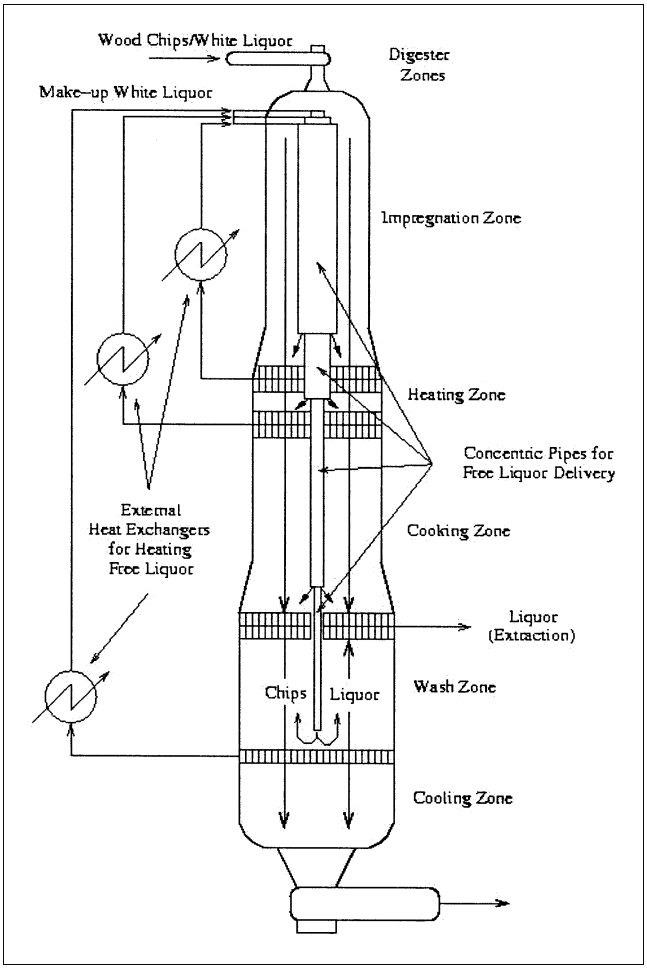

Figure 1. Single vessel continuous digester.

Smith and Williams (1974) developed kinetic models to describe delignification of chips based on the following form

$$R_{s,i} = -\left[k_{1,i}(T)C_{\mathrm{OH}}^{a} + k_{2,i}(T)C_{\mathrm{OH}}^{b}C_{\mathrm{HS}}^{c}\right](C_{s,i} - C_{s,i}^{\infty}) \quad (1)$$

where the temperature dependence of the rate constants are calculated using the Arrhenius law

$$k_{i,j}(T) = A_{i,j}\exp\left(\frac{-E_{i,j}}{RT}\right) \quad (2)$$

The wood substance was classified as high reactive lignin (s_1), low reactive lignin (s_2), cellulose (s_3), galactoglucomman (s_4), and araboxylan (s_5). Indices i and j refer to the two rate constants and the five solid components in the wood chips, respectively. Model constants (a, b, c, $A_{i,j}$, $E_{i,j}$) were evaluated by trial and error using pulping chemistry data. Smith and Williams then approximated the digester by a series of continuous stirred tank reactors (CSTRs) to obtain dynamic mass balances for the main components participating in pulping reactions. Each CSTR was assumed to contain three phases: (1) a solid phase consisting of the wood substance; (2) an entrapped liquor phase comprising of liquor in the pores of the wood chips; (3) a bulk free liquor phase surrounding the wood chips. The resulting digester model is referred to as the Purdue model. The major contribution of the Purdue model was the development of a framework upon which subsequent models could be based. Christensen et al. (1982) modified the Purdue model by incorporating improved kinetic parameters (based on an optimization search) valid over a larger range of wood species. The improved model predicted free liquor concentration profiles and blow-line Kappa # for an industrial digester, where the Kappa # is defined as follows

$$\text{Kappa \#} = \frac{\rho_{s_1} + \rho_{s_2}}{0.00153\left(\sum_{i=1}^{5}\rho_{s_i}\right)} \quad (3)$$

ρ_{s_i} (kg/m^3) refers to the concentration of the ith component of the wood solid. Gustafson et al. (1983) developed alternate kinetic expressions to describe the delignification reaction. They use a lesser number of wood and liquor components, and make use of functional relationships between the rate of consumption of carbohydrates and lignin. Greater emphasis is paid to penetration of liquor inside the chips.

Kayihan et al. (1996) presented a Weyerhaeuser benchmark model for a two-vessel Kamyr digester with separate impregnation and reaction vessels. The model assumed two phases: nonporous solid and free liquor, which exist in thermal equilibrium. The kinetic model of Christensen et al. (1982) was adopted to describe dynamic mass balances. The resulting set of partial differential equations (PDEs) is discretized spatially and the model is solved as a system of ordinary differential equations (ODEs). Extensions of the Purdue model have been presented by Wisnewski et al. (1997). They redefined mass concentrations and volume fractions that allowed relaxation of certain assumptions in the previous Purdue model leading to higher model fidelity. The extended Purdue model compared favorably and captured the range of behaviors displayed by the original Purdue model, as well as the Weyerhaeuser benchmark 2-vessel digester model.

In all of the preceding works, a steady, unchanging compaction profile is assumed. Further, these models fail to provide a dynamic description of chip level, an important control variable. This is a necessary consequence of absence of momentum transport modeling. On the other hand, hydraulic description based models in literature assume simpler chemistry, constraining the validity to narrower ranges of Kappa #. Härkönen (1987) presented a detailed description of chip and liquor flow dynamics, and compaction, in addition to mass and energy transport. Constitutive equations that described flow resistance were developed experimentally. The resulting model was a system of two-dimensional PDEs that were solved at steady state. Simplifying assumptions were made with regards to the reaction kinetics, and delignification in wood chips is ignored. Nevertheless, Härkönen's work laid the foundation for integrating digester hydraulics with existing models based on mass and energy transport. Michelsen (1995) proposed an integration of the works by Christensen et al. (1982) and Härkönen (1987) to develop a detailed digester model from mass, energy, and axial momentum transport balances. The model assumes solid, entrapped liquor and free liquor phases in the digester, and is described by a com-

plex set of algebraic equations and PDEs. It is solved numerically using a staggered grid finite difference approach. While chip and liquor flow dynamics are described in detail, simplifications are made in reaction kinetics, which constrain the validity of the model for Kappa # within the range of 50 and 150. A key result of Michelsen's model was ability to study the effect of flow behavior and compaction on Kappa #. Further, the study suggested residence time control could yield improved Kappa # control.

The model developed in this article is a direct integration of the works of Wisnewski et al. (1997) and Michelsen (1995) that overcomes some of the deficiencies described above. Thus, the detailed kinetics and mass/energy transport of the industrially established extended Purdue model are augmented with Michelsen's momentum transport description, yielding a thermal-hydraulic model of the continuous digester. Incorporation of momentum allows rigorous simulation of phenomena distinguished by interactions between the flow mechanics of the chips and free liquor and the delignification kinetics. Specifically, the current work provides the following capabilities over and above the Extended Purdue Model (Wisnewski et al., 1997): (a) rigorous simulation of production rate changes; (b) rigorous simulation of feedstock grade transitions; (c) ability to simulate chip level transients; and (d) simulation of incipient plugging of digester.

Each of these enhancements represents important characteristics of mill operation. Grade and rate transitions have assumed increasing significance in pulping mills necessitated by optimal production scheduling and planning policies. Chip level in the digester is strongly correlated with the quality of the pulp as it contributes to the retention time of chips in the digester. Digester plugging results in production downtime and represents a fault situation with serious economic consequences. The current work also represents significant improvements over the model by Michelsen (1995). Unlike the detailed pulping chemistry models (Christensen et al., 1982) used in the current work, Michelsen lumped chip components into lignin and carbohydrate. Also, the white liquor components were lumped into effective alkali and dissolved solids. Further simplifications were made in the kinetic rate expressions, which restrain the kinetic model validity to middle Kappa # ranges of 150 to 50. Justification of these assumptions was made on the grounds of development of a qualitative model. Use of Michelsen's (1995) model for predictive capability is limited owing to the fact that most mills cook chips to Kappa #s below 50. The following section presents the current thermal-hydraulic Purdue model and develops the model equations including a brief discussion on numerical issues. Next, a preliminary model validation result is provided with data from a U.S. domestic pulping mill. The model features are illustrated through simulations and parametric sensitivity followed by an extension of the model to simulate grade transitions. Finally, the work is summarized and further utility of the model is discussed.

Model Derivation

The proposed model is based on a distributed parameter approach, where the axial distribution of transport properties occurs due to the convection of the chips and liquor streams. The entry and exit of external streams, wall, and cross-flow effects (such as at extraction screen and heater inlets and outlets) are likely to cause radial gradients in temperature and concentration profiles (He et al., 1998). However, all radial gradients are neglected as a simplifying assumption. The temporal variations within each infinitesimal control volume are described by conservation statements, resulting in a set of coupled nonlinear PDEs. External flows from heaters and extraction screens are modeled as flows entering and/or leaving the control volume. The remainder of the section outlines the transport equations and constitutive rules used. The nomenclature and definitions used in the present document closely follow that of Wisnewski et al. (1997).

Physical description

As in the Purdue model, each control volume is assumed to contain three phases: solid phase, entrapped liquor phase, and free liquor phase. The entrapped liquor phase resides within the pores of the wood chips where it reacts with the solid substance. However, dynamic and thermal equilibria are assumed between these two phases. In this work, the combined solid and entrapped liquor phases will be referred to as the chip phase. An infinitesimal slice of the digester with volume ΔV is shown in Figure 2. The results presented later assume control volumes (CVs) with fixed cross-sectional areas A. An inventory of each phase at a fixed vertical location z in the digester is measured using the following volume fraction definitions

$$\eta = \frac{\text{volume of free liquor phase in } \Delta V}{\text{volume of } \Delta V}\left[\frac{\Delta V_f(z)}{\Delta V(z)}\right] \quad (4)$$

The remainder of the control volume is assumed to be occupied by the chip phase. Thus

$$(1-\eta) = \frac{\text{volume of chip phase in } \Delta V}{\text{volume of } \Delta V}\left[\frac{\Delta V(z)}{\Delta V_c(z)}\right] \quad (5)$$

The compaction profile along the length of the digester is influenced by the volumetric flow rates of the chip and free liquor phases, as well as the degree of cooking. The extended

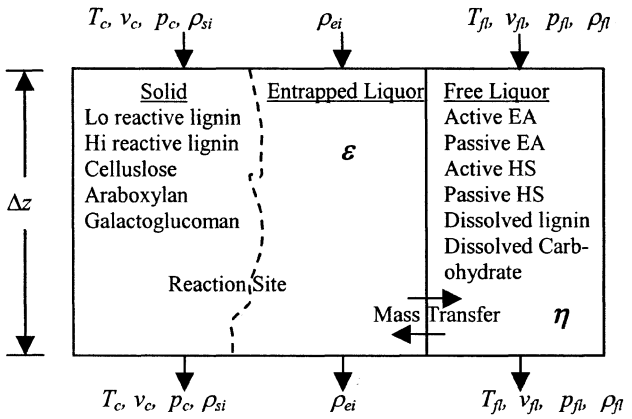

Figure 2. Cross-sectional slice of digester (cook zone) consists of solid, entrapped liquor and free liquor phases.

Purdue model assumed the compaction profile to be a fixed parameter of the model. The current work explicitly models chip compaction. Since chip phase volume consists of the solid wood substance and entrapped liquor, one can define the fraction of the chip phase occupied by entrapped liquor as the chip porosity

$$\epsilon = \frac{\text{volume of entrapped liquor phase in } \Delta V}{\text{volume of chip phase in } \Delta V}\left[\frac{\Delta V_e(z)}{\Delta V_c(z)}\right] \quad (6)$$

Equivalently

$$(1-\epsilon) = \frac{\text{volume of solid phase in } \Delta V}{\text{volume of chip phase in } \Delta V}\left[\frac{\Delta V_s(z)}{\Delta V_c(z)}\right] \quad (7)$$

As shown in Figure 2, the chip phase enters the digester slice with volumetric flow rate $\dot{V}_c(z)$ and exits at a rate of $\dot{V}_c(z+\Delta z)$. Free liquor flows cocurrently, with the chip phase, in the cooking zone and countercurrently in the wash zone. Volumetric flow of free liquor is defined by $\dot{V}_f$. Chip and free liquor phase velocities v_c and v_f are defined using, respectively

$$\dot{V}_c = A(1-\eta)v_c$$
$$\dot{V}_f = A\eta v_f \quad (8)$$

Specie concentrations employed in the conservation equations make use of definitions formulated by Wisnewski et al., as opposed to the earlier versions of Purdue model. The solid component concentration is defined on a chip volume basis as follows

$$\rho_{s,i} = \left[\frac{\text{mass of solid component } i \text{ in chip}}{\text{chip volume}}\right] \quad (9)$$

Similarly, for entrapped and free liquor concentrations, respectively

$$\rho_{e,i} = \left[\frac{\text{mass of entrapped liquor component } i \text{ in chip}}{\text{entrapped liquor volume in chip}}\right] \quad (10)$$

$$\rho_{f,i} = \left[\frac{\text{mass of free liquor component } i}{\text{free liquor volume}}\right] \quad (11)$$

Solid phase mass continuity

The solid phase is assumed to consist of five components: high-reactive lignin (s_1); low-reactive lignin (s_2); cellulose (s_3); araboxylan (s_4); and galactoglucomannan (s_5). Physical transport, as well as the rate at which they react with the liquor, determines the reactant concentrations. Performing a component balance for the solid phase at location z yields the following

$$\frac{\partial \rho_{s,i}}{\partial t} = -v_c\frac{\partial \rho_{s,i}}{\partial z} + \hat{R}_{s,i} \quad (12)$$

where $\rho_{s,i}$ is defined in Eq. 9. $\hat{R}_{s,i}$ represents the rate of consumption of mass of solid i per chip volume. The reaction rate used in the current work is based on the kinetic model developed by Christensen et al. (1982)

$$\hat{R}_{s,i} = -e_f\left(k_{1,i}\,\rho_{e,1} + k_{2,i}\,\rho_{e,1}^{1/2}\,\rho_{e,3}^{1/2}\right)\left(\rho_{s,i} - \rho_{s,i}^{\infty}\right) \quad (13)$$

where e_f is the reaction rate effectiveness factor. As discussed later, the main use of the effectiveness factor lies in tuning the model outputs to observed digester behavior. $\rho_{s,i}^{\infty}$ denotes the concentration of solid component i entering the digester, which is inert. Reaction rate constants $k_{1,i}$ and $k_{2,i}$ are determined using the Arrhenius law. Values of kinetic parameters for hardwood and softwood are summarized in Wisnewski et al. (1997).

Entrapped liquor phase mass continuity

It is assumed that the chips are saturated with water upon entering the digester. The water then mixes with reactants from free liquor that diffuse into the entrapped liquor and the dissolved reaction products from the solid phase. The entrapped liquor is, thus, an aqueous solution with six components: active effective alkali (EA) (e_1); passive EA (e_2); active hydrosulfide (HS) (e_3); passive HS (e_4); dissolved lignin (e_5), and dissolved carbohydrates (e_6). The entrapped liquor components are consumed during delignification of the solids and replenished in the cook zone by the free liquor via diffusion. A component balance yields

$$\frac{\partial \rho_{e,i}}{\partial t} = -\frac{\rho_{e,i}}{\epsilon}\frac{\partial \epsilon}{\partial t} - \frac{v_c}{\epsilon}\frac{\partial(\epsilon\rho_{e,i})}{\partial z} + D\left(\rho_{f,i} - \rho_{e,i}\right) + \hat{R}_{e,i} \quad (14)$$

$\rho_{e,i}$ represents concentration of entrapped liquor components defined as a mass of component i in an elementary control volume per entrapped liquor volume (see Eq. 10). The porosity of chips $\epsilon(z)$ is computed by comparing the density of solid-phase components defined on a chip volume basis with a density of solid wood substance $\bar{\rho}_s$ as follows

$$\epsilon(z,t) = 1 - \frac{\sum_{i=1}^{5}\rho_{s,i}(z,t)}{\bar{\rho}_s} \quad (15)$$

The third term on the righthand side of Eq. 14 models the diffusion of component i from the free liquor phase to the entrapped liquor phase. Early Purdue developers (Smith and Williams, 1974; Christensen et al., 1982) derived the following correlation for the mass diffusion rate (defined on a volume basis) D using experimental data for Kraft cooking presented in McKibbins (1960)

$$D = 6.1321\sqrt{T_c}\,\exp\left(\frac{-4{,}870}{1.98T_c}\right)\left[\frac{1}{\text{min}}\right] \quad (16)$$

Simulation results presented later are based on this correlation. Reaction rates $\hat{R}_{e,i}$ and $\hat{R}_{s,i}$ are related via stoichiometric coefficients $b_{i,j}$

$$\hat{R}_{e,i} = \sum_{j=1}^{5} b_{i,j}\hat{R}_{s,j} \quad (17)$$

The boundary conditions for the solid and entrapped phase continuity equations are fixed by the wood specie and the degree of impregnation.

In their work, Wisnewski et al. (1997) assume that the solids react and dissolve into the entrapped phase, contributing only mass and not volume. The newly created volume then draws in free liquor from the neighboring free liquor phase. This assumption violates volume continuity needed for calculation of compaction η and free liquor volumetric flow rates $\dot{V}_f$. Thus, only the diffusive mechanism is retained as the means of mass transfer from the free liquor to the entrapped phase. Since, the entrapped liquor phase is incompressible, neglecting the vacuum effect amounts to assuming that the reacted solid components retain their density as in unreacted form in the solid phase.

Free liquor phase mass continuity

The free liquor phase is an aqueous solution of the same six components, as in the entrapped liquor phase. Apart from bulk transport along the digester, free liquor concentrations are determined by the rate of diffusion to the entrapped liquor and mixing with external liquor streams. A component balance around the infinitesimal control volume gives the following

$$\frac{\partial \rho_{f,i}}{\partial t} = -\upsilon_c \frac{\partial \rho_{f,i}}{\partial z} - D\epsilon \frac{(1-\eta)}{\eta}(\rho_{f,i} - \rho_{e,i}) \pm \rho_{f,i,\text{ext}} \frac{\dot{V}_{\text{ext}}}{\Delta V_f} \tag{18}$$

Subscript ext refers to external streams (for example, heater circulation streams). The positive sign in the last term refers to external flows entering the control volume and negative for exiting flows. $\rho_{f,i}(z)$ represents concentration of component i per volume of free liquor (see Eq. 11). The rate of diffusion of free liquor to entrapped phase is equal to that entering the entrapped phase in Eq. 14, but expressed on a free liquor volume basis. The boundary conditions for the free liquor continuity equations are provided by the concentrations of white liquor components in the cook zone and concentration of wash liquor components in the wash zone.

Chip and free liquor thermal energy balances

Wisnewski et al. (1997) use mixing rules based on weighted averages to determine heat capacities of the entrapped and free liquor phases, namely, C_{Pe} and C_{Pf}, respectively. The same approach is retained in the current work.

Below, energy balance equations, modified to accommodate variable compaction, are presented for the chip and free liquor phases, and describe the temporal variation of the chip phase temperature T_c and free liquor temperature T_f

$$(C_{Ps}M_s + C_{Pe}M_e\epsilon)\frac{\partial T_c}{\partial t} = -T_c\left(C_{Ps}\frac{\partial M_s}{\partial t} + C_{Pe}\frac{\partial (M_e\epsilon)}{\partial t}\right) - \upsilon_c \frac{\partial}{\partial z}\left[(C_{Ps}M_s + C_{Pe}M_e\epsilon)T_c\right] + \Delta H_R \sum_{i=1}^{5} \hat{R}_{s,i} + U(T_f - T_c) + D\epsilon D_{\text{E}} \tag{19}$$

Heat released by the exothermic reactions between the entrapped liquor and solid-phase components is modeled using the heat of reaction ΔH_R. The heat-transfer coefficient U models the convective heat transfer between the chips and free liquor phases. D_E represents the amount of energy transferred due to diffusion of components between the entrapped liquor and free liquor phases. The direction of diffusion is dependent on the concentration gradient. Thus

$$D_E = \sum_{i=1}^{4} (\rho_{f,i} - \rho_{e,i})C_{P_f}T_i + \sum_{i=5}^{6} (\rho_{f,i} - \rho_{e,i})C_{PS}T_i \tag{20a}$$

where

$$T_i = \begin{cases} T_f & \text{if } \rho_{f,i} > \rho_{e,i} \\ T_c & \text{if } \rho_{f,i} < \rho_{e,i} \end{cases} \tag{20b}$$

A similar balance for the free liquor phase yields

$$C_{Pf}M_f\frac{\partial T_f}{\partial t} = -T_f\frac{\partial}{\partial t}(C_{Pf}M_f) - \upsilon_f\frac{\partial}{\partial z}(C_{Pf}M_fT_f) - U\frac{(1-\eta)}{\eta}(T_f - T_c) - \frac{D\epsilon(1-\eta)D_E}{\eta} \pm \frac{\dot{V}_{\text{ext}}M_{\text{ext}}T_{\text{ext}}}{\Delta V_f} \tag{21}$$

The term $[D\epsilon(1-\eta)D_E]/\eta$ represents the energy transfer with the chip phase per volume of diffusing mass. The last term represents the energy transfer due to bulk motion of incoming/exiting external streams. Temperatures of wood chip charge, entering white liquor and entering wash liquor temperatures, fix the boundary conditions needed for Eqs. 19 and 21. Equations 1–21 are based on the work by Wisnewski et al. (1997), but modified to account for chip compaction and momentum balances. The reader is referred to that work as the source for all parameters and constants (for example, values of heat-transfer coefficient, diffusion coefficient, and so on) used in the simulation results presented in the next section.

Chip phase volume continuity

As discussed previously, progressive cooking of chips cause them to soften, thereby changing shape, but not volume. The only mechanism that affects compaction of chips in a given control volume is the convective flows of chip phase and liquor. Thus, a volume balance for the elemental volume ΔV yields the following compaction equation

$$\frac{\partial \eta}{\partial t} = \frac{\partial}{\partial z}\left[(1-\eta)\upsilon_c\right] \tag{22}$$

The compaction equation is central in providing insights to incipient digester plugging discussed later. Michelsen's model includes axial dispersion in addition to convective flow of chips. However, subsequent steady-state analysis shows that the dispersion has a negligible effect on compaction. Michelsen also makes a degree of freedom argument to demonstrate how volume continuity follows from mass continuity. The boundary conditions for Eq. 22 are fixed by compaction of chips in a top section.

Overall digester volume continuity

Equation 22 provides information on the fraction of the control volume occupied by chips. To satisfy overall digester volume continuity, the remainder of the volume must be occupied by free liquor. This, in turn, prescribes the volumetric flow rate of free liquor as follows

$$\nabla_z\left(\dot{V}_c + \dot{V}_f\right) = 0 \tag{23}$$

where the incoming and exiting external flows are included in the liquor flow rate. Equation 23 is a static constraint expressing incompressibility of the contents of a control volume in the digester. It states that the sum of all flow rates entering a control volume of fixed size equals the sum of all flow rates exiting the volume. In the extended Purdue model (Wisnewski et al., 1997), bulk flow of free liquor into the entrapped phase by the vacuum effect decreases the flow rate of the exiting free liquor stream. However, no corresponding volume increase occurs in the chip phase thereby violating the incompressibility assumption. We assume that the rate of extraction of the liquors from the cook and wash zone is perfectly controlled. These values are then used to compute the volumetric flow distribution using Eq. 23.

Pressure distribution in the free liquor phase

The free liquor pressure distribution $p_f(z)$ is mainly dictated by the hydrostatic head in the digester. Depending on the degree of cooking, the chip phase at a given location z has a certain Kappa # associated with it. Härkönen (1987) performed experimental studies to evaluate the effect of cooking on the compactability of chips and then defined a chip pressure p_c, which is the force that acts through the interchip contact points over a reference area. As noted by Michelsen (1995), the chips become softer during cooking enabling them to pack more tightly. The softening of chips is reflected by reduced chip pressure. Härkönen's (1987) work also suggests that, while the chips become softer during cooking, they change shape but no appreciable change in volume occurs. Calculation of the free liquor pressure distribution in presence of liquor velocity transients is a nontrivial task. Iterative methods (ex. SIMPLE algorithm, Patankar (1980)) exist in literature, which simultaneously arrive at a distribution of pressure and velocity fields such that the momentum and continuity equations are satisfied. However, the approach used here is to neglect free liquor momentum dynamics and utilize the resulting momentum equation to prescribe the pressure distribution. Michelsen (1995) suggests that this approach may be reasonable, since the period of free liquor velocity transients will be short due to incompressibility implied by Eq. 23.

Various forces affecting the system determine the free liquor pressure. Given the large capacity and height of the digester, gravity plays an important role in determining the liquor pressure. The remainder of the forces arises as a result of the viscous resistance faced by the chips, as they flow through the liquor phase with a non-zero relative velocity. Härkönen (1987) developed expressions for the resistive force based on the Ergun equation. He defined the resistive force as

$$F_\Lambda = \Lambda v_{c,f} \tag{24}$$

where the coefficient of viscous friction is

$$\Lambda = R_1\frac{(1-\eta)^2}{\eta} + R_2(1-\eta)|v_{c,f}| \tag{25}$$

and $v_{c,f}$ is the relative velocity between the chip and liquor phases. R_1 and R_2 are parameters estimated from experimental data. The pressure distribution is calculated as

$$\frac{\partial p_f}{\partial z} = -v_f\frac{\partial}{\partial z}[\rho_f v_f] + \rho_f g + \frac{F_\Lambda}{\eta} \tag{26}$$

The axial liquor pressure distribution is primarily determined by the forces of gravity and the chip-liquor interphase friction. The first term on the righthand side of Eq. 26 describing momentum convection is relatively small and may be omitted. The digester is assumed to be completely filled with liquor with a fixed pressure on the top. Equation 26 then provides the liquor pressure in the remainder of the digester column.

Chip phase velocity distribution

In addition to the interphase flow resistance, Härkönen (1987) also used experimental data to model the chip pressure discussed previously as a function of degree of cooking measured by Kappa # and compaction of chips η follows

$$p_c = 10^4\left(\frac{(1-\eta)-0.356}{\alpha - 0.139\ln(\text{Kappa }\#)}\right)^{1.695} \quad \text{if } (1-\eta) < 0.356$$
$$= 0, \qquad \text{otherwise} \tag{27}$$

where the parameter α has a nominal value of 0.831 based on experimental data. The equation is based on the cross-sectional area of the digester. For chip compaction below 35.6%, the chips float freely and do not exert pressure on adjacent chips. For a fixed compaction, the chip pressure decreases with increased cooking. The physical interpretation of decreasing chip pressure is that the chips become softer during cooking (reflected by decrease in Kappa #) due to increased porosity. The softening mechanism with increased cooking is modeled as decrease in chip pressure. The softening of chips enables tighter packing of chips thereby decreasing the volume fraction of chips. Thus, decrease in chip pressure is accompanied with decreasing volume fraction of chips.

Härkönen (1987) models the force of sliding friction between the chip phase and the digester walls as

$$F_\mu = \frac{4\mu p_c}{D_{cv}} \tag{28}$$

where μ is the coefficient of sliding friction and D_{cv} represents the diameter of the digester cross-sectional area. Using Newton's second law and combining the above forces, we get

the axial chip velocity distribution as follows

$$\rho_c(1-\eta)\frac{\partial v_c}{\partial t} = -v_c(1-\eta)\rho_c\frac{\partial v_c}{\partial z} + \rho_c(1-\eta)g - \frac{\partial p_c}{\partial z} - (1-\eta)\frac{\partial p_f}{\partial z} - F_\Lambda - F_\mu \quad (29)$$

As before, contribution of convective momentum is small relative to other forces. Pulp production rate in the blow-line fixes the boundary condition for the chip momentum equation. The coefficient of viscous friction, chip pressure, and the coefficient of sliding friction in Eqs. 25, 27 and 28, respectively, are determined empirically. Further experimental work is necessary to determine their accuracy in different operating ranges.

Chip level

Chip level constitutes one of the most important variables in digester control. It impacts the Kappa # via residence time of the chips in the digester. To model chip level, a top section of the digester is assumed, which covers a certain volume over the impregnation zone and consists of the chip phase interface. Chip phase inventory description then provides the dynamic description of level

$$\dot{h}_c = \frac{1}{A(1-\eta_{\text{top}})}\left[\dot{V}_{c,\text{feed}} - A(1-\eta_0)v_{c,0}\right] \quad (30)$$

where η_{top} is an estimate of the compaction in the top section. Michelsen (1995) suggests using a linear relationship between the chip level and η_{top}

$$(1-\eta_{\text{top}}) = \begin{cases} 0.356 & \text{if } h_c < h_{\min} \\ 0.356 + k_{ts}h_c & \text{otherwise} \end{cases} \quad (31)$$

where $h_{\min}$ represents a reference height of the chip plug. η_{top} also forms the boundary condition for Eq. 21. Note that variables related to the bottom of the top section are indexed with zero, implying the beginning of the main section of the digester. The coefficient k_{ts} is determined empirically. Equations 22 through 31 are primarily based on works by Härkönen (1987) and Michelsen (1995).

Numerical method

For solution purposes, the model PDEs are replaced with a finite difference mesh on a digester grid, such as shown in Figure 3. Notation j refers to a fixed grid node on the digester vessel with the jth control volume lying between nodes $j-0.5$ and $j+0.5$. Note that continuity balances are performed at half nodes while momentum balances for chip and liquor phase are performed at node j with $j-0.5$ and $j+0.5$ as the control volume boundaries (see Figure 3). This overlapping of mass and momentum control volumes leads to a staggered grid approach and is routinely used in numerical fluid flow problems (Patankar, 1980). The approach ensures that only reasonable (nonwavy) pressure distributions are acceptable as solutions. In the current model, axial transport of properties in the digester occurs by convection alone, resulting in a system of hyperbolic PDEs. It is well known that solutions based on finite differences distort the information

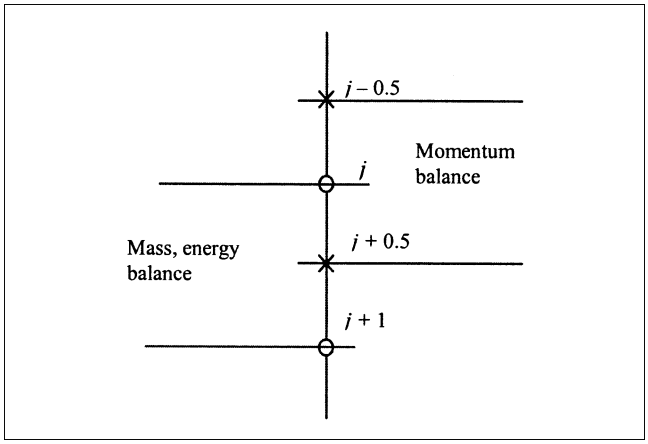

Figure 3. Arrangement of overlapping control volumes in digester vessel.

that is being convected downstream (Anderson et al., 1984). For example, simulation of a step-like change upstream of a flow system will exhibit dissipation or dispersion due to the truncation errors in the finite difference scheme, regardless of the modeling assumptions (see Figure 4). To study the impact of the truncation errors, the spatial derivatives were differenced using two different schemes, namely upstream differencing

$$\frac{du_i}{dz} = \frac{u_i - u_{i-1}}{h} + O(z) \quad (32)$$

and a fourth-order difference formulation

$$\frac{du_i}{dz} = \frac{-u_{i-3} + 6u_{i-2} - 18u_{i-1} + 10u_i + 3u_{i+1}}{12h} + O(z^4) \quad (33)$$

where h represents the height of the finite control volume. Simulation results presented in the next section make use of the first-order formula. An assessment of using the higher-order formula is presented separately.

Preliminary Model Validation

A preliminary model validation exercise was performed using real data from a large U.S. domestic pulping mill. The mill in question uses a two-vessel Kamyr digester. The two vessels (impregnation vessel and digester vessel) were divided

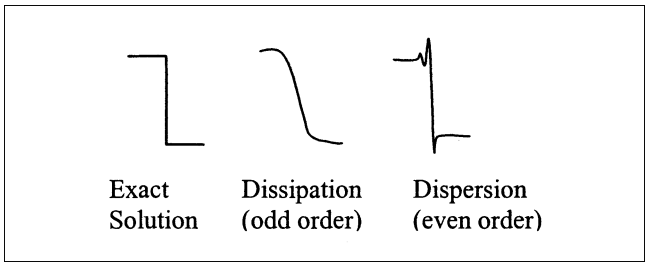

Figure 4. Finite differences inducing numerical diffusion.

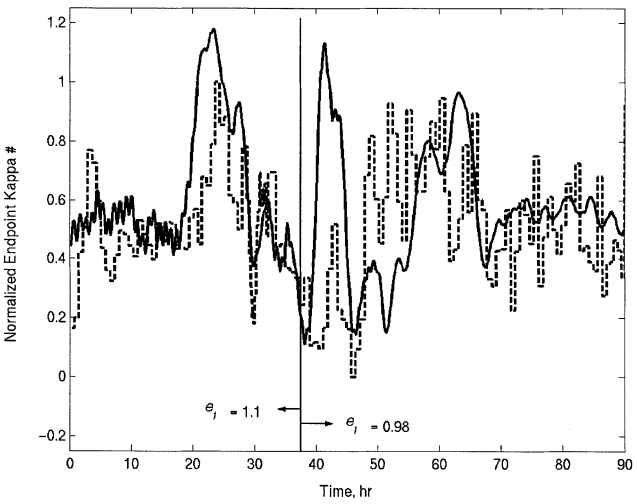

Figure 5. Preliminary model validation using real data from a large U.S. domestic mill.

Dashed line represents mill measurements of digester endpoint Kappa #. The solid line is the corresponding model prediction.

into 118 control volumes and Eqs. 1–32 were implemented. PI controllers were implemented to control the chip levels in the two vessels using the respective upstream chip flow rates as the manipulated variable. The model was tuned using historic data from the mill DCS. The aim of model tuning was achieving a similar predicted endpoint Kappa # and predicted residual effective alkali at the extraction screen to the mill measurements. However, no attempt was made to validate the various constitutive rules (for example, kinetic rate constants and the coefficient of friction) due to lack of appropriate data. Rather, the values documented by Wisnewski et al. (1997) and Michelsen (1995) were adopted. The reaction rate effectiveness factor e_f of Eq. 13 constituted the primary tuning knob. Details of the vessel dimensions were obtained from the vessel drawings and mapped to the model. The model inputs constituted mill measurements of the chip meter RPM (volumetric flow rate of raw chips), pulp production rate, and the flow rates and temperatures of the various liquor streams, sampled at a 10 min interval. The tuned model was validated with approximately 90 h of mill operation. Comparison of the model prediction of the digester endpoint Kappa # with scaled mill measurements is shown in Figure 5.

The reaction rate effectiveness factor e_f was manually switched from an initial value of 1.1 to a new value of 0.98 after approximately 37 h of operation. This parameter scales the kinetic model, thereby directly determining the extent of conversion or the Kappa #. The excursion in the predicted Kappa # between 37 and 46 h is a result of the instantaneous switching of the model parameter. Over the course of the 90 h period, four different production rate transitions were implemented at the mill, which covered a substantial range of production rates. The need for a change in e_f may be attributed to a number of factors. Large changes in the production rate, as in the current case, or operating space, in general, are likely to affect model parameters. Further, various unmeasured inputs such as the concentration of solid components of the naturally occurring wood, and wood chip moisture, exhibit stochastic variations. These factors can potentially lead to drifts in the digester base line conditions over long periods of operation necessitating changes in model parameters for long-term model fidelity. Suitably designed estimators must, therefore, accompany use of the model in online applications such as model predictive control and process monitoring. These estimators will likely ensure a smoother change in the parameters, thereby eliminating the spurious bump observed between 37 and 46 h in Figure 5. Although the current validation exercise is preliminary (only one model parameter identified from mill data by trial and error method, chip level controllers in model at variance with mill controllers), trends in the model predictions of the endpoint Kappa # follow those of mill measurements. Also, the values of the predicted endpoint Kappa # are in proximity to the mill measurements, except during the period immediately following switching of the parameter e_f.

Simulation Results and Discussion

The simulations presented in this section are based on operating parameters presented in Table 5 in Wisnewski et al. (1997). The digester was divided into 96 control volumes and Eqs. 1–31 were implemented using Matlab/Simulink on a Sun Sparc Ultra 10, 333 MHz workstation. Table 1 summarizes the locations of the heater and extraction screen. Inclusion of momentum conservation makes the system relatively stiff. However, computational burden is alleviated by the use of the sparsity pattern of the Jacobian matrix. A typical run simulating 80 h of digester operation requires about 17 min of real time.

Steady-state behavior

A direct benefit of including momentum in the extended Purdue model is ability to simulate production rate changes. Figure 6 shows comparisons between steady-state profiles of various digester variables for a low production rate (LPR) at 1.328 m^3/min and a high production rate (HPR) of pulp at 1.478 m^3/min (dashed line). The blow-line flow rate step change was implemented using a first-order filter with a time constant of 13 min. A simultaneous step change was introduced in the chip flow rate at top of the digester. This was necessary due to the integrating behavior of level dynamics. The reduced residence time of chips leads to lower extent of conversion of lignin (Figure 6a) and a corresponding increase in Kappa # profile (Figure 6f). The Kappa # for both the cases shows an initial increase in the impregnation zone ($z <$ 0.14) due to rapid consumption of araboxylan relative to lignin. Subsequently, the Kappa # decreases in the cooking zone ($0.14 < z < 0.75$), beyond which the reaction is quenched by the cooler and dilute wash liquor. Figures 5b–5d show components of entrapped and free liquor. The increase in

Table 1. Control Volumes in the Different Zones of Digester

Digester Zone	No. of Control Vol.
Impregnation	17
Upper heater	7
Lower heater	7
Cooking	41
Wash	24

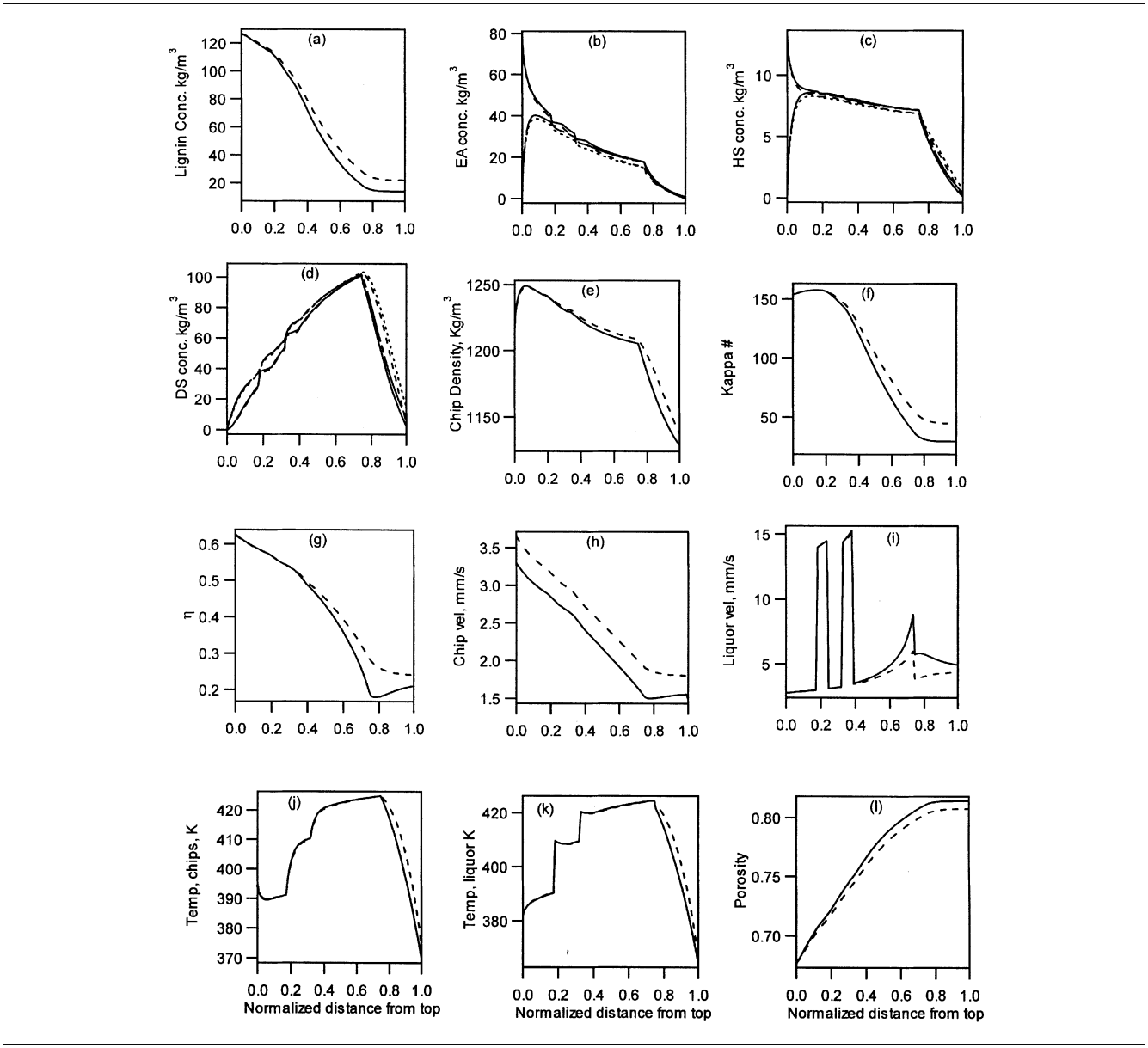

Figure 6. Steady-state behavior for low (solid) and high (dashed) blow-line flow rates.

Impregnation zone: $z < 0.14$; cook zone: $0.14 \leq z < 0.75$; wash zone: $z \geq 0.75$.

blow-line flow for the HPR case reduces available time for diffusion of EA and HS from free liquor to the entrapped phase leading to a drop in concentrations in the entrapped phase. However, this increases the concentration driving force, which in turn causes the free liquor concentrations to drop as well. These figures also illustrate that the use of the correlation in Eq. 16 for calculation of diffusion coefficient leads to near-equilibrium conditions between the free and entrapped liquors. Volume fraction of liquor for the HPR case (Figure 6g) increases near the extraction screen, implying loose packing of chips. This is a result of a lower degree of cooking or higher Kappa #, and is consistent with the argument that a greater degree of cooking leads to denser packing of chips. The higher value of η results in lowering of liquor velocities (Figure 6i), as more area is available for the free liquor flow. The increase in chip velocity (Figure 6h) is a result of higher volumetric throughput. Figures 6j and 6k show the temperatures of chip and liquor along the length of the digester. Chip porosity profiles are shown in Figure 6l. Chip porosity increases in the direction of chip flow as the solid components are progressively consumed. Relatively lower porosity is observed for the HPR simulation due to lower extent of delignification.

Dynamic response

Dynamic behavior of the digester is characterized by large dead times in primary measurements, such as the endpoint Kappa #. Incorporation of digester hydraulics involves the relatively fast response variables of chip and liquor velocities.

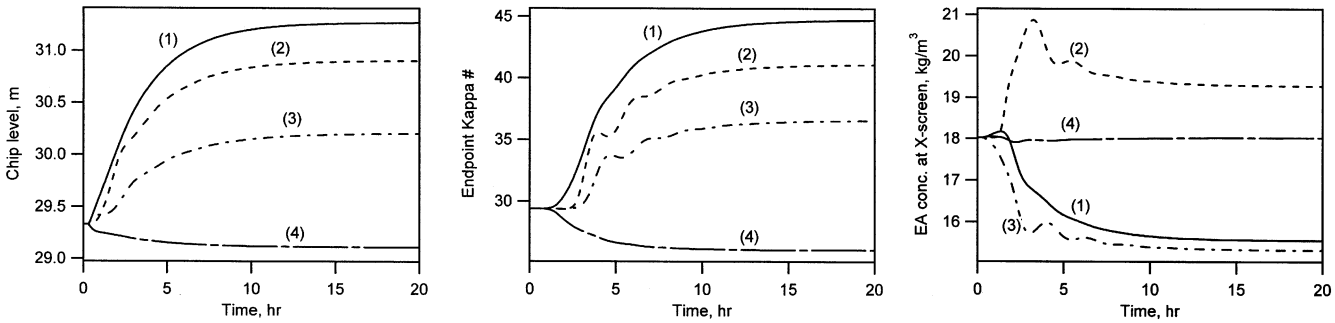

Figure 7. Dynamic behavior for: (1) increase in blow-line flow; (2) decrease in upper heater temp.; (3) decrease in white liquor; (4) decrease in dilute liquor flow.

Changes in liquor flow rates are instantaneously propagated in direction of flow due to the static nature of Eq. 23. This difference in time-scales introduces stiffness in the model. Figure 7 shows results for filtered step changes in: (1) blow-line flow; (2) cooking circulation upper heater; (3) white liquor, (4) dilute liquor flows of 0.15 m^3/min, -10°C, -0.15 m^3/min, and -0.15 m^3/min, respectively. In each of the cases, the relation between the endpoint Kappa # and chip level is apparent, as they are coupled via residence time. Cases 1 and 3 result in lower cooking due to a lower rate of availability of chemicals, while lower cooking in case 2 is due to a lesser amount of energy. The decrease in the chip level in case 4 is due to the lower "lift" provided by the reduced dilute liquor flow rate. In each of the four cases, changes in levels are due to rearrangement of the chip compaction profile. Cases 2 and 3 show kinks and oscillatory behavior in the endpoint Kappa # plot while traversing from the initial steady state to the final steady state. No simple mechanistic explanation emerges from the dynamic equations. Upon an analysis of simulations, it is observed that the oscillations first appear in the Kappa # and chip velocity when the upper heater temperature is perturbed (Figure 8). The initial increase in Kappa # is accompanied by a retardation of chip velocity due to increased chip pressure, which propagates downstream giving rise to the oscillatory behavior in the Kappa #. Increasing numerical tolerances does not cause this behavior to disappear. Figure 9 shows comparisons for steps in white liquor and dilute liquor flows in opposite directions. Increase in white liquor amounts to increased availability of chemicals and therefore more cooking. For opposite directions of the same-sized step, the process gains are seen to be nonlinear.

Incipient digester plugging

Strong interactions between the mass/energy conservation and the hydraulic features enable simulation of a fault scenario in the digester with serious adverse economic consequences, namely, plugging of the digester. The momentum equation interacts with the model kinetics through the chip pressure gradient, which is a function of the Kappa and compaction profiles. The resulting interaction between the Kappa # and chip velocity was evident in Figure 8. Simulation studies reveal that at lower Kappa numbers, chip compaction $(1 - \eta)$ can significantly increase and chip velocities decrease near the extraction screens forming a plug (see Eq. 22). Chip velocities in the digester usually reduce spatially from the top of the digester to the extraction screen (for example, see Figure 6h). The corresponding softening of the chips increases chip pressure gradient, a negative driving force of the chip velocities in Eq. 29. Also, increasing flow resistance reduces the value of η. Since $\eta = 0$ results in a singularity, only incipient plug formation can be observed (very small values of η), at which point the equations become extremely stiff and the simulation slows down considerably. As an example, steady-state compaction and Kappa # profiles for a filtered step increase in white liquor flow rate are shown in Figure 10. Excessive cooking nearly causes the digester to plug up near the extraction screen. This is the result of dense packing of

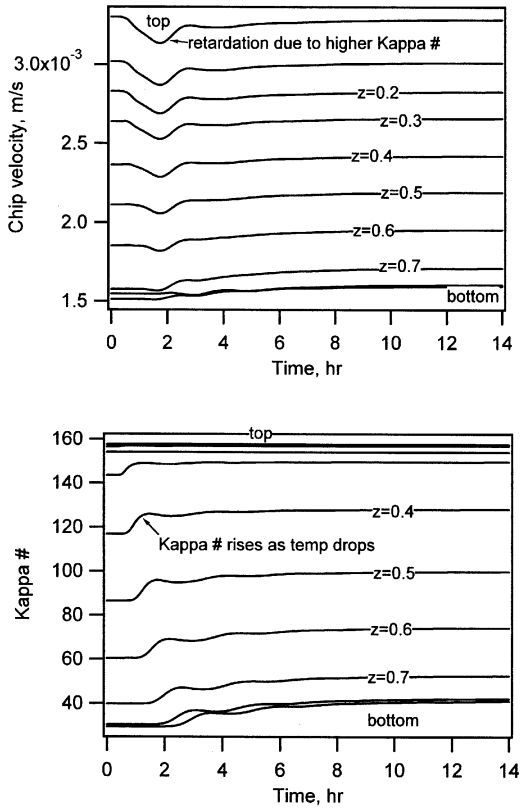

Figure 8. Velocity and Kappa # transients at various locations on the digester due to change in upper heater circulation temperature.

"Top" and "bottom" refer to the digester.

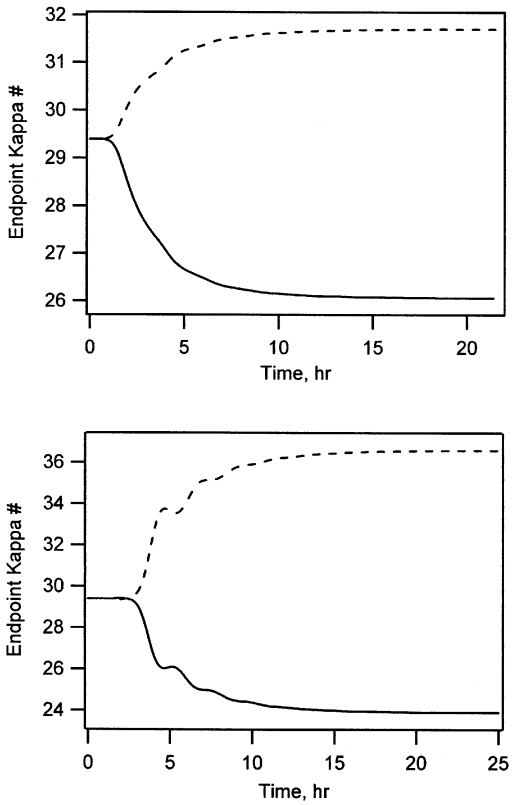

Figure 9. Symmetric step tests for: (a) ± 0.15 m^3/min change in dilute liquor flow; (b) ± 0.15 m^3/min change in white liquor flow.

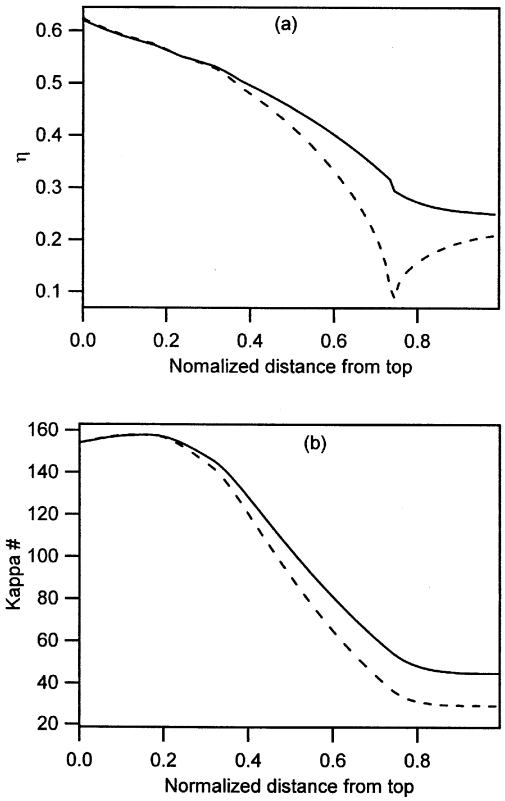

Figure 10. Steady-state compaction and Kappa # profiles for low (solid) and high (dashed) values of white liquor flow rates.

Sharp kink in the compaction profile (dashed) corresponding to higher white liquor flow represents incipient plugging in the digester.

cooked chips ($< 2\%$ free liquor) near the extraction screen. The counter flow of dilute liquor aids in dispersing the fibers as the pulp enters the wash zone.

As discussed in the next section, the plugging behavior is sensitive to the parameters in the chip pressure Eq. 27. It is possible to eliminate the plugging behavior for the same operating conditions and chips cooked to nearly the same endpoint Kappa # by changing parameters of the chip pressure equation. While the potential for plugging the digester, when cooked to lower Kappa numbers, is encountered in the industry, it may be necessary to perform experiments to further investigate the impact of the chip pressure term on this important fault condition.

Model parameter sensitivity analysis

Wisnewski et al. (1997) studied model sensitivity to various parameters in the heat- and mass-transfer equations. Similar trends were observed with the current thermal-hydraulic Purdue model and corresponding results are, therefore, omitted. Only model sensitivity to some key parameters in the momentum equations is discussed. Figure 11a shows steady-state compaction profiles for two different values of the parameter α in Eq. 27. Reducing the value of α to 0.816 from the nominal value of 0.831 increases the value the fraction of liquor η from 0.08 to 0.18, implying a lowering of chip compaction at the extraction screen. As discussed in the last section, a very small value of η can be interpreted as incipient plugging of the digester. The corresponding Kappa # profile is shown in Figure 11b, where the endpoint Kappa # increases by about 3. Thus, the value of the parameter α plays an important role in determining axial distribution of chip compaction in the digester, while affecting the Kappa # profile only marginally.

Figure 12 shows the velocity and compaction profiles when parameter R_2 in Eq. 25 is varied by 30% in either direction. An increase in R_2 leads to increased flow resistance, thereby decreasing chip velocities. Consequently, chip compaction rearranges itself by decreasing area available for chip flow (by increasing η) to satisfy overall chip continuity. Reducing R_2, on the other hand, increases has an opposite effect. Negligible changes are observed in the Kappa # profile. A similar observation is made with flow resistance related parameters R_1 and μ in Eqs. 25 and 28, respectively.

Assessment of higher-order numerical method

To study the impact of using a higher-order numerical method on variables of interest, such as endpoint Kappa #, the following experiment was performed. The simulation based on the first-order difference method (Eq. 32) was allowed to reach steady state after which the fourth-order scheme (Eq. 33) was used without changing any operating conditions or model parameters. Figure 13 depicts the re-

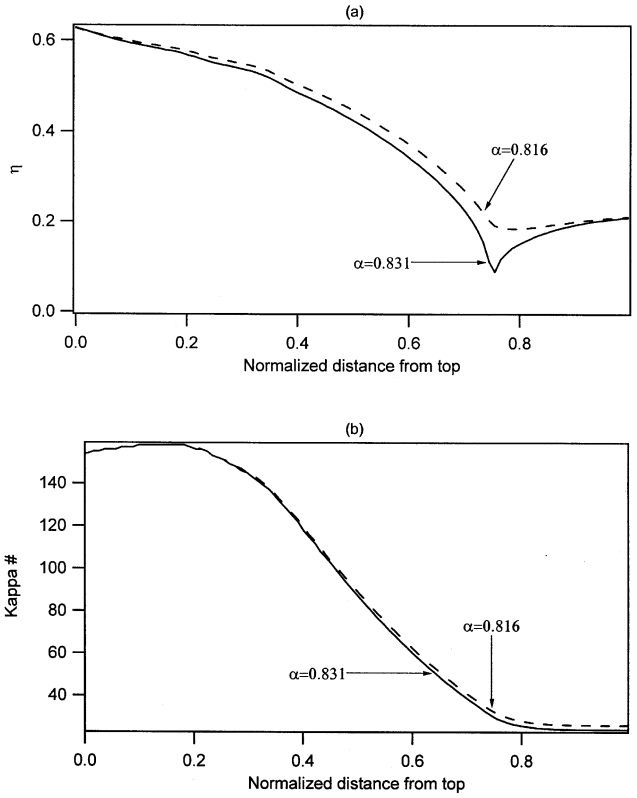

Figure 11. Sensitivity of (a) chip compaction and (b) Kappa # to changes in parameter α in Eq. 27.

While no substantial change is observed in the Kappa # profile, the chip compaction shows chip compaction is lowered when α is changed from the nominal value of 0.831 to 0.816, implying easier drainage of chips.

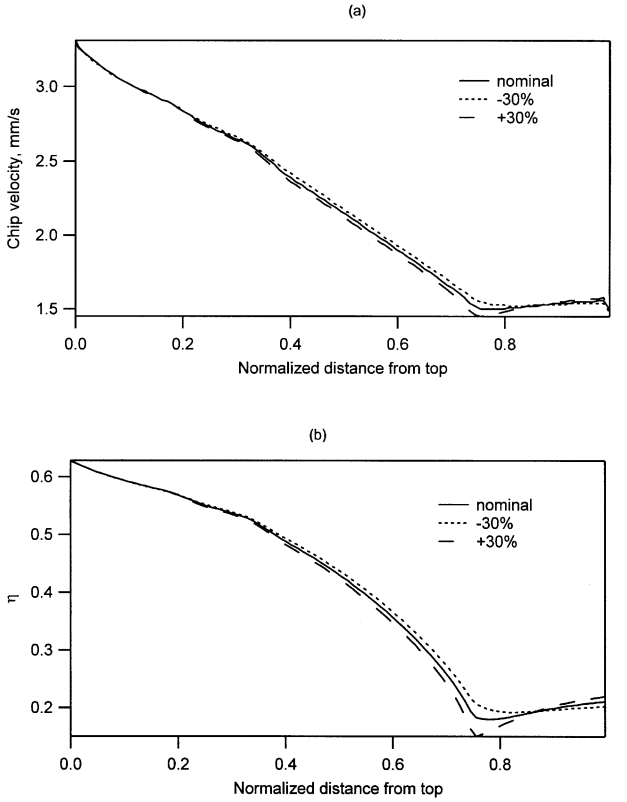

Figure 12. Model sensitivity to change in parameter R_2 in Eq. 25.

(a) Increasing R_2 increases flow resistance and, hence, causes a decrease in velocity; (b) to maintain the same volumetric flow rate, a corresponding decrease in η is observed.

sults. It is noted that the higher-order formulation predicts increased conversion of lignin leading to a drop in Kappa # by about 3. Use of the first-order method approximates the digester as a series of CSTRs. However, chip flow in the digester more closely resembles plug flow since backmixing is absent. It is known that the CSTR usually accomplishes lower conversion for a given volume than the plug-flow reactor (Fogler, 1999). Thus, the increased conversion with the higher-order method is consistent with the fact that the fourth-order finite difference formula provides a better approximation of the plug-flow behavior in the digester. However, use of the fourth-order method decreases system sparsity and increases stiffness resulting in increased computation time. Thus, the first-order method is retained in all future simulations.

Grade Transition Modeling

Pulping mills often switch the feedstock grade from hardwood to softwood and vice versa to satisfy demands from the downstream paper machine section. There are frequent changes from one feedstock species to other commonly performed in the pulp industry. Of particular interest is the reduction of off-spec "twilight" pulp produced during the transition achieved by an effective grade transition policy. Industrial experience indicates that minimizing blending of the feedstock grades at the feed results in "good" transitions. Christensen et al. (1982) incorporated capability to simulate hardwood/softwood swings by empirically calculating the transition front between the two grades. Their model switched the old grade kinetic parameters to the new grade parameters as the old grade depleted from a finite difference volume

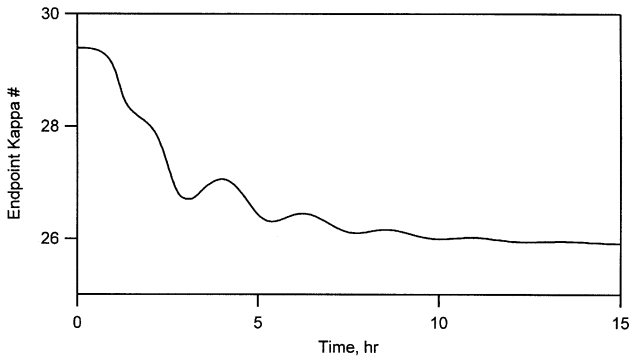

Figure 13. Higher-order numerical method predicting higher removal of lignin from chips.

Initial conditions correspond to steady-state conditions with a first-order finite difference formulation. At $t = 0$, the convective flow of chips is described by a 4th-order formulation with all operating parameters unchanged.

and filled with the new grade. The model performed well when compared to swing data. Doyle et al. (2001) modified the extended Purdue model to simultaneously accommodate both hardwood and softwood species in the same section of the digester. This was achieved by redefining certain mass concentrations and introducing a mixing parameter distributed along the length of the digester. The mixing parameter served as a first-order filter which allowed a smooth change in the mass fraction between the two species. However, the model did not account for digester hydraulics.

The current work follows the idea of a discrete transition front as in the Purdue model by Christensen et al. However, unlike their use of an empirical calculation of the grade transition front, momentum conservation allows calculation of the transition front using rigorous fundamental principles. The model assumes that a discrete transition front enters the top of the digester and proceeds downwards. Location of the transition front is calculated by integration of the front velocity obtained from the chip velocity distribution in the digester

$$\frac{dz_0}{dt} = v_c(z = z_0) \tag{34}$$

All kinetic parameters upstream of z_0 are switched to new grade properties, while old grade parameters are retained downstream. Properties within the control volume with the transition front are volume averaged based on the location of the front. Thus, the filtering capability similar to Doyle et al. (2001) exists in the vicinity of the front.

Figure 14 shows Kappa # profile snapshots at different times during a feed transition from softwood to hardwood. The grade swing was obtained with an open-loop operating policy that involved decreasing the upper and lower heater temperatures from 429 K to 416 K and 443 K to 424 K, respectively, as the front location z_0 reached the respective heater locations. Also, the white liquor flow rate to the top of the digester was decreased by 40% after the transition front crossed the extraction screens. Current industrial practices also make similar appropriate open-loop manipulations based on the front location estimated using the chip meter speed. It

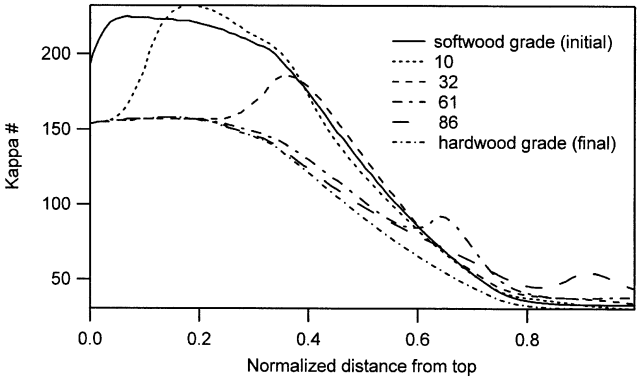

Figure 14. Kappa profile with the softwood to hardwood transition front at different locations.

Numbers in the legend refer to the control volume in which the front lies when the snapshot is taken. Appropriate changes were made to the heater temperatures to achieve acceptable endpoint Kappa numbers.

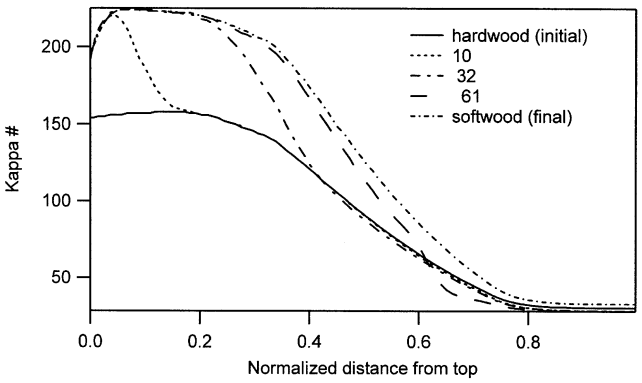

Figure 15. Kappa profile for hardwood to softwood transition.

Numbers in the legend refer to the control volume in which the front lies when the snapshot is taken.

is observed that, in a softwood to hardwood transition, the reduction in the energy and cooking chemicals, in anticipation of the reduced lignin content of the new grade, results in lower cooking (or higher Kappa #) during the transition time. On the other hand, transition of the feedstock grade from hardwood to softwood presented in Figure 15, involves increasing temperatures and white liquor flow rates during transition. These actions tend to overcook the remainder of the hardwood grade during transition. Simulation studies show that if the heater temperatures and white liquor flow rates are changed aggressively, the consequent overcooking may result in incipient plugging of the digester. This is consistent with the industrial experience that transition from hardwood to softwood is operationally more difficult than vice versa. Unlike the softwood to hardwood transition, the temperatures were increased here only after 30 min elapsed after the transition front completely crossed the respective heater locations. White liquor flow was increased after the transition front crossed the extraction screen. Simulations with heater temperature changes when the front crossed the respective heater location led to the incipient plugging phenomena described earlier. Endpoint Kappa # transients during the two grade transitions depicted in Figures 14 and 15 are shown in Figure 16. The undershoot in the hardwood to softwood transition represents the overcooking of the older hardwood grade. This overcooking takes place despite the 30 min. delay in increasing the heater temperatures as discussed above. If the heater temperatures are increased as soon as the front reaches the respective heater location, considerable overcooking (endpoint Kappa # drops to 15 before increasing) and the associated plugging problem are observed. Figure 17 shows the dynamic trajectory of the front location as the hardwood species completely fills the digester. Both the transitions are similar, with softwood to hardwood transition occurring more quickly than the hardwood to softwood transition.

Conclusions

In the paper and pulp industry, there are vast incentives to reduce off-specification pulp during operation. Unlike the refining industry, very limited blending opportunities exist to

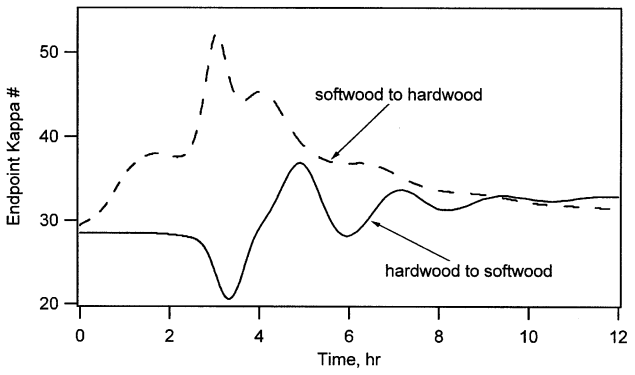

Figure 16. Digester endpoint Kappa number transients for grade change transitions.

Increase in heater temperatures during the hardwood to softwood transition overcooks the exiting hardwood grade leading to the undershoot in the endpoint Kappa #.

produce good quality end-products after production of pulp. A detailed fundamental model can aid in operational improvements using optimization to evaluate open-loop strategies during production rate and grade transitions. It can also be used to perform system identification and control. Wisnewski and Doyle (1998) show improved control performance using reduced extended Purdue model in comparison to purely data-driven models using model predictive control. However, previous versions of the Purdue model ignored momentum transport, an important element of digester operation. In this work, a thermal-hydraulic model of the continuous digester has been presented. The model provides a detailed description of the important phenomena involved in operating the digester using conservation laws. Constitutive rules were adopted from available literature (Christensen et al., 1982; Härkönen, 1987). Pulping chemistry was based on the Purdue model, while the hydraulics mainly rely on work by Härkönen (1987). Thus, the work constitutes a hydraulic extension of the Purdue model. The model illustrates that interactions between the kinetics and hydraulics play an important role in plugging of the digester vessel.

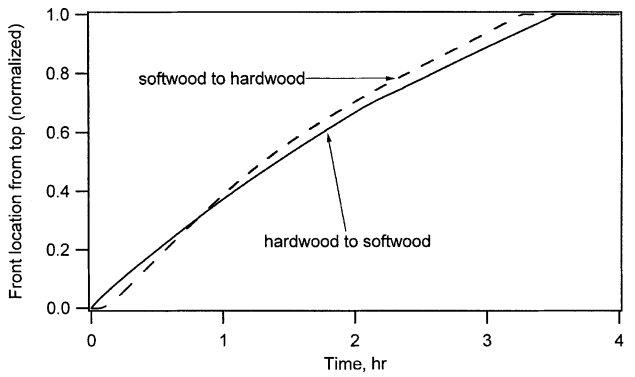

Figure 17. Dynamic trajectory of transition front for the two cases of grade transition.

Grade transition is modeled by assuming a discrete transition front. Kinetic parameters upstream of the front are switched to values for the new grade, while old grade parameters are retained downstream.

Simulation examples demonstrated various attributes of the model. While no rigorous validation exercise was performed, the variable trends follow those of the extended Purdue model (Wisnewski et al., 1997), where applicable, and can be explained mechanistically. The preliminary validation results using data from a U.S. domestic mill indicates realistic model predictions. The benefits of the hydraulic extension, however, are realized in the ability of the model to explain the impact of dynamic flow rate and compaction changes on the pulp quality. Moreover, the chip level, an important control variable, is one of the model outputs. Parametric sensitivity revealed that occurrence of incipient digester plugging was strongly related to parameters in the chip pressure equation. Further experimental investigations are necessary to confirm this observation. Incorporation of momentum transport also allows a straightforward extension to modeling grade transitions. An explicit tracking of the transition front allows switching of kinetic parameters. A key contribution lies in demonstrating operational difficulties encountered during a feedstock grade change. It is demonstrated that hardwood to softwood requires delayed changes in heater temperatures and white liquor flow rates to avoid overcooking.

Acknowledgment

The authors gratefully acknowledge funding from the Department of Energy (Grant DE-FC07-00ID-13882), MeadWestvaco Company, and Weyerhaeuser Company.

Notation

A = cross-sectional area of digester, m^2
$A_{i,j}$ = preexponential factors for ith rate constant during consumption of jth solid component, $m^3/(s \cdot kg)$
$b_{i,j}$ = stoichiometric coefficients for consumption of white liquor components, OH and HS
C_{ps}, C_{pe}, C_{Pf} = specific heat capacity of solid, entrapped liquor and free liquor phases, $J/(kg \cdot K)$
D = coefficient of diffusion, s^{-1}
D_{cv} = diameter of digester, m
D_E = energy transported by diffusion into entrapped liquor, J/m^3
e_f = reaction rate effectiveness factor
$E_{i,j}$ = activation energy for ith rate constant during consumption of jth solid component, $J/(mol \cdot K)$
F_Λ = viscous force of friction between chip and liquor phases, N/m^3
F_μ = force of sliding friction between chip phase and vessel, N/m^3
ΔH_R = heat of reaction, J/kg
$k_{i,j}$ = ith kinetic rate constant for consumption of jth solid component, $m^3/(s \cdot kg)$
M_s, M_e, M_f, M_{ext} = mass of solid, entrapped and free liquor phases, and external stream, kg
p_c = chip pressure, Pa
p_f = free liquor pressure, Pa
$R_{s,i}$ = reaction rate of solid component i, kg/s
$R_{s,i}$ = specific reaction rate of solid component i, kg/s
R = universal gas constant, $J/(mol \cdot K)$
T_c, T_f = temperature of chips and free liquor, K
T_{ext} = temperature of external stream, K
U = interphase heat-transfer coefficient, $J/(s \cdot m^3 \cdot K)$
$\dot{V}_c(z,t), \dot{V}_f(z,f)$ = volumetric flow rate of chips and free liquor at axial location z and time t, m^3/s
$\dot{V}_{ext}$ = volumetric flow rate of external stream, m^3/s
v_c, v_f = velocities of chip and free liquor phases, m/s
$v_{c,f}$ = velocity of chips relative to free liquor phase, m/s
$\Delta V(z)$ = volume of control volume, m^3

ΔV_e, ΔV_f = volumes of entrapped and free liquor phases in control volume, m^3

ΔV_s, ΔV_c = volumes of solid and chip phase in control volume, m^3

ϵ = fraction of chip phase occupied by entrapped liquor, or porosity

η = fraction of control volume occupied by free liquor

μ = coefficient of sliding friction

$\rho_{e,i}$ = concentration of ith component of entrapped liquor phase, kg/m^3

$\rho_{f,i}$ = concentration of ith component of free liquor phase, kg/m^3

$\rho_{f,i_{\text{ext}}}$ = concentration of ith component in external stream, kg/m^3

$\rho_{s,i}$ = concentration of ith component of solid phase, kg/m^3

$\rho^{\infty}_{s,i}$ = concentration of ith component of solid phase which does not react, kg/m^3

ρ_c, ρ_f = overall density of chip phase and free liquor phase, kg/m^3

Literature Cited

Anderson, D. A., J. C. Tannehill, and R. H. Pletcher, *Computational Fluid Mechanics and Heat Transfer*, McGraw Hill, New York (1984).

Christensen, T., L. F. Albright, and T. J. Williams, "A Mathematical Model of the Kraft Pulping Process," Tech. Rep. 129, PLAIC, Purdue University, West Lafayette, IN (1982).

Doyle, F. J., L. Puig, and F. Kayihan, "Grade Transition Modeling in Continuous Pulp Digester for Reaction Profile Control," *Pulp & Paper Canada*, **102**, 56 (2001).

Fogler, H. S., *Elements of Chemical Reaction Engineering*, 3rd ed., Prentice Hall, NJ (1999).

Gustafson, R., C. Sleicher, W. McKean, and B. Finlayson, "Theoretical Model of the Kraft Pulping Process," *Ind. Eng. Chem. Proc. Des. Dev.*, **22**, 87 (1983).

Härkönen, E. J., "A Mathematical Model for Two-Phase Flow in a Continuous Digester," TAPPI J., **70**, 122 (1987).

He, P., M. Salcudean, I. Gartshore, and E. L. Bibeau, "Modeling of Kraft Two-Phase Digester Pulping Processes," TAPPI Conf., Anaheim, CA (1998).

Kayihan, F., M. S. Gelormino, E. M. Hanczyc, F. J. Doyle III, and Y. Arkun, "A Kamyr Continuous Digester Model for Identification and Controller Design," *Proc. IFAC World Cong.*, San Francisco, Elsevier Science Publishers, New York, p. 37 (1996).

McKibbins, S. W., "Application of Diffusion Theory to the Washing of Kraft Cooked Chips," *Tappi J.*, **43**, 801 (1960).

Michelsen, F. A., "A Dynamic Mechanistic Model and Model-Based Analysis of a Continuous Kamyr Digester," PhD Thesis, University of Trondheim, Norway (1995).

Patankar, S., *Numerical Heat Transfer and Fluid Flow*, McGraw Hill, New York (1980).

Smith, C. C., and T. J. Williams, "Mathematical Modeling, Simulation and Control of the Operation of Kamyr Continuous Digester for Kraft Process," Tech. Rep. 64, PLAIC, Purdue University, West Lafayette, IN (1974).

Wisnewski, P. A., F. J. Doyle III, and F. Kayihan, "Fundamental Continuous Pulp Digester Model for Simulation and Control," *AIChE J.*, **43**, 3175 (1997).

Wisnewski, P. A., and F. J. Doyle III, "Control Structure Selection and Model Predictive Control of the Weyerhaeuser Digester Problem," *J. Proc. Control*, **8**, 487 (1998).

Manuscript received Apr. 10, 2002, and revision received Aug. 27, 2002.